Journal of Sound and Vibration (2001) **243**(4), 721–745
doi:10.1006/jsvi.2000.3430, available online at http://www.idealibrary.com on IDEAL®

ON GEARED ROTORDYNAMIC SYSTEMS WITH OIL JOURNAL BEARINGS

S. Theodossiades and S. Natsiavas

Department of Mechanical Engineering, Aristotle University, 54006 *Thessaloniki, Greece.*
E-mail: natsiava@ccf.auth.gr

(*Received* 26 *May* 2000, *and in final form* 29 *September* 2000)

This study investigates response and stability characteristics of rotordynamic systems interconnected with gear pairs and supported on oil journal bearings. The systems examined are driven by a motor providing a known torque, which is transferred to a load element through shafts and a gear box. Initially, the emphasis is placed on the gear-pair action, by assuming that the interconnecting shafts are rigid. This results in low order mechanical models with strongly non-linear characteristics, whose long-time dynamics are then effectively studied by applying appropriate numerical methodologies. In this way, useful information is obtained about the influence of the loading, the gear mesh and the journal parameters on the system dynamic behaviour, including periodic, quasi-periodic and chaotic response. Efforts are also directed towards predicting the onset of oil whirl instability and investigating its effects on the system dynamics. The focus is then shifted to more realistic models, including the flexibility of the interconnecting shafts. In this case, the order of the system is first reduced by applying a component mode synthesis method, which takes advantage of the fact that the non-linearities are located at the journal bearings and the gear mesh only. As a result, it is possible to study the dynamics of the reduced rotor-bearing model by employing the methodology that was developed for the gear-pair models.

1. INTRODUCTION

Geared rotor-bearing systems have found extensive application as power transmission elements in many engineering applications. The continuously rising technological needs for improved performance, compactness, longer life and reduced production costs, require new designs with higher operating speeds and lighter components. In order to satisfy these needs, research in the area of geared systems has remained active, incorporating new technical advancements and theoretical developments in other related fields. These efforts are also greatly assisted by current rapid enhancements in the level of computing power, which in turn extends the range of applicability of numerical algorithms involved. As a result, a large number of publications have appeared in the literature, dealing with simple gear-pair systems as well as with more involved gear trains (see references [1–9] and references therein).

Previous studies on geared rotor-bearing systems have addressed many important technical issues, such as the effect of support and gear box flexibility, gyroscopics, internal and external damping, shaft shear deformation and gear meshing properties on their coupled torsional-bending vibrations. The great majority of these studies assume constant average spin speed of the gear shafts. As a consequence, the errors in the gear tooth profile and spacing as well as the mass and moment unbalance act as external excitation on the system, together with the applied torques. Both response and stability issues have been

0022-460X/01/240721 + 25 $35.00/0

investigated by means of analytical, numerical and experimental techniques. Among all the technical parameters, those related to the gear backlash and the variable gear meshing stiffness were found to affect the system response significantly. As a result, their effects have been re-examined in more depth and detail in some recent studies (e.g., references [6–9]). Finally, parameters related to stiffness and damping properties of the supporting journal bearings were also found to play an equally important role [10].

In the simpler case of single-shaft rotordynamic systems, much progress has been reported on the effect of oil journal bearings on several response and stability issues [10–15]. For instance, in one of the most recent studies on the subject [15], the steady state response of a single-shaft system was determined by applying an effective numerical methodology, combining component mode synthesis [16, 17] and determination of periodic solutions by the finite difference and a path continuation method [18, 19]. This study verified that for some parameter combinations, a periodic motion may lose stability when the rotor spin speed is about 2 times the lowest natural frequency of the corresponding linearized system. As a result, a new, asynchronous motion is developed, known as oil whirl or whip and characterized by much higher response amplitudes than the coexisting synchronous unstable periodic motion [13].

Some studies have also appeared on dual- and multi-shaft systems supported by oil journal bearings (e.g., references [20–26]). In particular, a study of a marine steam turbine, with a two-stage reduction gear system, supported on journal bearings and subjected to partial loading, reported an instability when the shaft spin speed approaches twice the frequency value of a torsionally dominated mode [20]. In other experimental results [21], it was concluded that the purely torsional gear models of a gas turbine-compressor train are not accurate and that the lateral–torsional coupled modes can be significantly suppressed by oil film dampers. In terms of analytical work, effects of journal bearings on the stability of a simple geared rotor system were examined in reference [22], while a rigid gear–rotor pair on oil film bearings under moment excitation was studied in reference [23]. Moreover, a six-degree-of-freedom gear-pair model with one shaft supported on a cavitated squeeze film damper was studied in reference [24]. Periodic motions were determined by the trigonometric collocation method for a gear mesh with constant stiffness and damping parameters and no backlash. Performing stability analysis also identified ranges of parameters where the periodic response loses stability and gives rise to a complex response [25]. Finally, some numerical results were recently obtained by direct integration for a similar gear-pair model, supported on short oil film bearings and engaged with gears involving time periodic mesh stiffness and no backlash [26].

The objective of the present work is to extend the previous research efforts in two principal directions. First, the emphasis is put on developing a systematic methodology for studying dynamics of gear-pair systems supported by hydrodynamic bearings. In the resulting models, in addition to the non-linearities introduced by the bearing action, the gears involve backlash and the gear mesh stiffness is expressed as a periodic function of the driving gear rotation. Such models are useful in gaining a better understanding on the interaction of the bearing and the gear meshing non-linearities, as well as on their influence on the overall system dynamics. The second objective is to present a methodology for the systematic and effective determination of the behaviour of complex geared rotor-bearing systems, with flexible shafts. This methodology involves a crucial step, leading to a substantial reduction of the original degrees of freedom, which in turn makes the application of efficient numerical methodologies feasible for predicting the system dynamics.

The organization of this paper is as follows. In the next section, a gear-pair model is developed, involving four lateral and two torsional degrees of freedom, coupled through the

forces developed in the oil film bearings and the gear mesh. The motion is caused by a motor unit, exerting a known external torque, which is transferred to a load unit, having a known torque resistance form. As a result of this approach, in addition to the non-linearities due to the bearing and the gear meshing forces, the gear static transmission error and the unbalance forcing appear also as non-linear terms in the equations of motion. Some of these difficulties are then overcome by adopting the classical assumption that, at steady state, the gear shafts rotate with a constant average spin speed. This approach is presented in section 3 and leads to a five-degree-of-freedom model, after proper elimination of one of the torsional degrees of freedom. In section 4, a general methodology is presented for the dynamic analysis of high order geared rotor-bearing models, by taking into account the gear shaft flexibility, through the application of finite element techniques. This method exploits the fact that the system non-linearities are related directly to relatively few degrees of freedom and reduces the order of the system without sacrificing much of the computational accuracy. Numerical results are then presented in sections 5 and 6, illustrating the influence of the system parameters on its dynamic response and stability. The final section includes a synopsis and the main findings of the study.

2. A GEAR-PAIR SYSTEM ON JOURNAL BEARINGS

The study focuses on geared rotordynamic systems, involving hydrodynamic bearings. Figure 1 shows a simple mechanical model, retaining the essential characteristics which arise from the interaction of the gear mesh and the bearing non-linearities. It consists of a spur gear pair, with equivalent mass m_i, polar moment of inertia I_i and base radius R_i. The driving gear ($i = 1$) is subjected to a known torsional moment M_1, while the driven gear ($i = 2$) develops a resistance moment M_2, with known form. Both gears are supported on plain oil journal bearings through rigid shafts. As a consequence, the motion of the system is

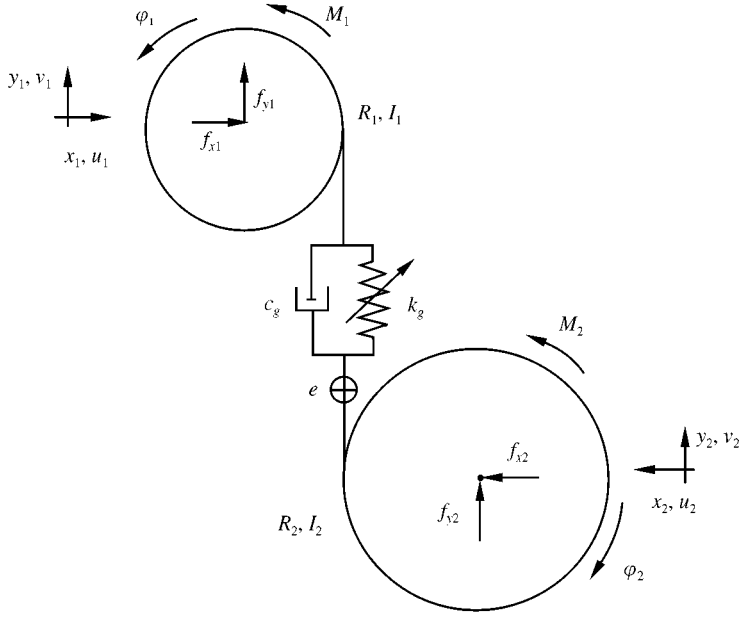

Figure 1. Mechanical model of a gear-pair.

described adequately by the following set of generalized co-ordinates

$$\mathbf{u}(t) = (u_1 \;\; v_1 \;\; \varphi_1 \;\; u_2 \;\; v_2 \;\; \varphi_2)^{\mathrm{T}}.$$

The corresponding equations of motion can initially be set in the general form

$$m_1\ddot{u}_1 + f_{x1}(u_1, v_1, \dot{u}_1, \dot{v}_1, \dot{\varphi}_1) = F_{x1}(t, \varphi_1, \dot{\varphi}_1), \tag{1}$$

$$m_1\ddot{v}_1 + f_{y1}(u_1, v_1, \dot{u}_1, \dot{v}_1, \dot{\varphi}_1) + f_g(\varphi_1, w, \dot{w}) = F_{y1}(t, \varphi_1, \dot{\varphi}_1), \tag{2}$$

$$I_1\ddot{\varphi}_1 + R_1 f_g(\varphi_1, w, \dot{w}) = M_1(t, \varphi_1, \dot{\varphi}_1), \tag{3}$$

$$m_2\ddot{u}_2 + f_{x2}(u_2, v_2, \dot{u}_2, \dot{v}_2, \dot{\varphi}_2) = F_{x2}(t, \varphi_2, \dot{\varphi}_2), \tag{4}$$

$$m_2\ddot{v}_2 + f_{y2}(u_2, v_2, \dot{u}_2, \dot{v}_2, \dot{\varphi}_2) - f_g(\varphi_1, w, \dot{w}) = F_{y2}(t, \varphi_2, \dot{\varphi}_2), \tag{5}$$

$$I_2\ddot{\varphi}_2 - R_2 f_g(\varphi_1, w, \dot{w}) = -M_2(t, \varphi_2, \dot{\varphi}_2), \tag{6}$$

where the composite co-ordinate

$$w = R_1\varphi_1 - R_2\varphi_2 + v_1 - v_2 - e(\varphi_1) \tag{7}$$

is the so-called dynamic transmission error. The definition of this quantity is related to the gear meshing action and assumes that the lateral displacements u_1 and u_2, which are normal to the line of action of the gear pair, have a negligible effect on it, when compared to the contribution of the displacements v_1 and v_2. In addition, this quantity includes the static transmission error, resulting from geometrical errors in the gear teeth profile and spacing. This error is a periodic function of the rigid-body rotation of the gears. Neglecting the tooth to tooth variations, it can therefore be expressed in the Fourier series

$$e(\varphi_1) = e(\varphi_1 + \varphi_{1T}) = e_0 + \sum_{p=1}^{\infty} [e_{cp}\cos(pn_1\varphi_1) + e_{sp}\sin(pn_1\varphi_1)] \tag{8}$$

with fundamental period equal to $\varphi_{1T} \equiv 2\pi/n_1$, where n_1 is the number of teeth in the driving gear.

In general, the driving torque M_1 is a known function of time as well as of the rotation angle φ_1 and its time derivatives, while the resisting moment M_2 is a function of time, the rotation angle φ_2 and its derivatives. Likewise, the terms F_{x1}, F_{y1}, F_{x2} and F_{y2} include the contribution of forces resulting from gravity and unbalance effects. Moreover, if the damping mechanism in the gear mesh is linear, the corresponding force is expressed in the form

$$f_g(\varphi_1, w, \dot{w}) = c_g\dot{w} + f_g(w)\,k_g(\varphi_1). \tag{9}$$

The restoring force developed at the gear meshing takes into account the variation of the gear mesh stiffness $k_g(\varphi_1)$, which is expressed in the form

$$k_g(\varphi_1) = k_g(\varphi_1 + \varphi_{1T}) = k_0 + \sum_{p=1}^{\infty} [k_{cp}\cos(pn_1\varphi_1) + k_{sp}\sin(pn_1\varphi_1)]. \tag{10}$$

In addition, the gear backlash is modelled by the piecewise linear function

$$f_g(w) = \begin{cases} w - b, & w \geqslant b, \\ 0, & |w| < b, \\ w + b, & w \leqslant -b, \end{cases}$$

where $2b$ represents the total gear backlash.

The terms f_{x1}, f_{y1}, f_{x2} and f_{y2} represent the forces developed at the journal bearings. These forces appear in several forms, depending on the bearing dimensions (i.e., length L,

diameter $D = 2R$ and radial clearance C_r). One of the most commonly applied methods in determining journal bearing forces is the finite-length impedance method [10], which determines the bearing hydrodynamic forces based on the gear centre position (u, v) and velocity $(\dot{u}, \dot{v})$, as well as on the angular speed $\dot{\varphi}$ of the gear. In brief, knowledge of these parameters initially permits the evaluation of the gear centre eccentricity ratio ε and inclination angle β, defined by

$$\varepsilon = \sqrt{u^2 + v^2}/C_r, \quad \cos\beta = u/\varepsilon C_r, \quad \sin\beta = v/\varepsilon C_r$$

(for a complete geometrical and physical interpretation of these and the following journal bearing quantities see reference [10]). By direct differentiation, these quantities yield the corresponding time derivatives $\dot{\varepsilon}$ and $\dot{\beta}$, which then allows the evaluation of the journal's pure-squeeze-speed

$$V_s = C_r \sqrt{\dot{\varepsilon}^2 + \varepsilon^2 (\dot{\beta} - \bar{\omega})^2} \quad \text{with} \quad \bar{\omega} = \dot{\varphi}/2.$$

Moreover, this leads to a direct calculation of the parameters

$$\cos\eta = (\dot{u} - \bar{\omega}v)/V_s, \quad \sin\eta = (\dot{v} + \bar{\omega}u)/V_s, \quad \alpha = \beta - \eta.$$

These values are, in turn, useful in determining an angle γ through the expression

$$\gamma = [1 - a(1 - b^2)^{-1/2}](\tan^{-1} A - \pi/2\ b/|b| + \sin^{-1} b) + \alpha - \sin^{-1} b,$$

where

$$A = 4(1 + 2{\cdot}12B)(1 - b^2)^{1/2}/3(1 + 3{\cdot}60B)b, \quad B = (1 - \varepsilon^2)(D/L)^2,$$

$$a = \varepsilon\cos\alpha \quad \text{and} \quad b = \varepsilon\sin\alpha.$$

Then, the impedance amplitude is evaluated from

$$W = [0{\cdot}15\,(E^2 + G^2)^{1/2}\ (1 - \xi)^{3/2}]^{-1}$$

with

$$E = 1 + 2{\cdot}12Q, \quad G = 3\eta(1 + 3{\cdot}60Q)/4(1 - \xi), \quad Q = (1 - \xi)(D/L)^2,$$

$$\xi = \varepsilon\cos\gamma \quad \text{and} \quad \eta = \varepsilon\sin\gamma.$$

Eventually, the journal bearing force is determined in the form

$$\mathbf{f}_b = 2\mu V_S L(R/C_r)^3\ \mathbf{W}, \tag{11}$$

where μ represents the oil viscosity coefficient and the components of the impedance vector $\mathbf{W}$ in the xy co-ordinate system are given by

$$W_x = W\cos\phi \quad \text{and} \quad W_y = W\sin\phi$$

with $\phi = \alpha - \gamma + \eta$.

Using the definition of the displacement vector $\mathbf{u}(t)$, the original set of equations (1)–(6) can be written in the compact form

$$\mathbf{M}\ddot{\mathbf{u}} + \mathbf{C}\dot{\mathbf{u}} + [k_g(\varphi_1)\, f_g(w) - c_g e'(\varphi_1)\dot{\varphi}_1]\mathbf{k} + \mathbf{f}_b\,(\mathbf{u}, \dot{\mathbf{u}}) = \mathbf{f}(t, \boldsymbol{\varphi}, \dot{\boldsymbol{\varphi}}), \tag{12}$$

where $\mathbf{M}$ is a diagonal matrix with elements m_1, m_1, I_1, m_2, m_2 and I_2, while

$$\mathbf{C} = c_g \begin{bmatrix} 0 & 0 & 0 & 0 & 0 & 0 \\ & 1 & R_1 & 0 & -1 & -R_2 \\ & & R_1^2 & 0 & -R_1 & -R_1R_2 \\ & & & 0 & 0 & 0 \\ & & & & 1 & R_2 \\ sym & & & & & R_2^2 \end{bmatrix}, \quad \mathbf{k} = \begin{pmatrix} 0 \\ 1 \\ R_1 \\ 0 \\ -1 \\ -R_2 \end{pmatrix}, \quad \mathbf{f}_b = \begin{pmatrix} f_{x1} \\ f_{y1} \\ 0 \\ f_{x2} \\ f_{y2} \\ 0 \end{pmatrix}, \quad \mathbf{f} = \begin{pmatrix} F_{x1} \\ F_{y1} \\ M_1 \\ F_{x2} \\ F_{y2} \\ -M_2 \end{pmatrix}$$

and $\boldsymbol{\varphi}(t) = (\varphi_1 \ \ \varphi_2)^{\mathrm{T}}$. For convenience in the numerical calculations, the set of equations (12) can be written in the normalized form

$$\tilde{\mathbf{M}}\ddot{\mathbf{v}} + \tilde{\mathbf{C}}\dot{\mathbf{v}} + \tilde{\mathbf{k}}(\psi_1, \hat{w}) + \tilde{\mathbf{f}}_b(\mathbf{v}, \dot{\mathbf{v}}) = \tilde{\mathbf{f}}(\tau, \boldsymbol{\psi}, \dot{\boldsymbol{\psi}}), \tag{13}$$

after introducing a characteristic length x_c and the dimensionless time $\tau = \omega_0 t$, where

$$\omega_0 = \sqrt{\frac{k_0}{m}} \quad \text{and} \quad m = I_1 I_2/(I_1 R_2^2 + I_2 R_1^2).$$

The quantities $\mathbf{v}(\tau)$, $\boldsymbol{\psi}(r)$ and $\hat{w}$ result after dividing $\mathbf{u}(t)$, $\boldsymbol{\varphi}(t)$ and w, respectively, by the characteristic length x_c.

3. AN ALTERNATIVE GEAR-PAIR MODEL

In more classical formulations, it is usually assumed that the gear rotation can be decomposed in the form

$$\varphi_i(t) = \omega_i t + \theta_i(t) \tag{14}$$

with $i = 1, 2$. That is, the total rotation angle of each gear consists of two distinct components. The first represents a rigid-body rotation, resulting from a mean angular speed ω_i of the gear shaft, so that $R_1\omega_1 = R_2\omega_2$. The second component includes small angular variations $\theta_i(t)$, caused by vibration of the mating gear teeth. Then, if the angular speeds ω_i are constant and the tooth-to-tooth variations are neglected, the static transmission error and the gear meshing stiffness terms can be expressed in a time Fourier series form, instead of equations (8) and (10). For instance,

$$k_g(t) = k_0 + \sum_{s=1}^{\infty} [p_s \cos(s\omega_M t) + q_s \sin(s\omega_M t)] = k_g(t + T_M)$$

with $T_M = 2\pi/\omega_M$, where $\omega_M = n_1\omega_1 = n_2\omega_2$ is the gear meshing frequency. Moreover, the static transmission error and the external torques become also periodic functions of time, with the same fundamental period T_M and without any dependence on the rotation co-ordinates or their derivatives.

Based on the new assumptions, equations (3) and (6) can be combined into a single equation

$$m(\ddot{w} - \ddot{v}_1 + \ddot{v}_2) + f_g(\varphi_1, w, \dot{w}) = F(t) \tag{15}$$

with

$$F(t) \equiv m[R_1 M_1(t)/I_1 + R_2 M_2(t)/I_2 - \ddot{e}(t)].$$

In this way, the rigid-body rotation of the system is eliminated from the equations of motion. In addition, making use of the last result, equations (2) and (5) may be replaced by

$$(m_1 + m)\ddot{v}_1 - m(\ddot{w} + \ddot{v}_2) + f_{y1}(u_1, v_1, \dot{u}_1, \dot{v}_1, \omega_1) = F_{y1}(t) - F(t) \tag{16}$$

and

$$(m_2 + m)\ddot{v}_2 + m(\ddot{w} + \ddot{v}_1) + f_{y2}(u_2, v_2, \dot{u}_2, \dot{v}_2, \omega_2) = F_{y2}(t) + F(t) \tag{17}$$

respectively. Consequently, the new set of equations of motion can eventually be written in the form

$$\mathbf{M}\ddot{\mathbf{u}} + \mathbf{C}\dot{\mathbf{u}} + \mathbf{k}(t, w) + \mathbf{f}_b(\mathbf{u}, \dot{\mathbf{u}}, \omega_1) = \mathbf{f}(t) \tag{18}$$

with

$$\mathbf{u}(t) = \begin{pmatrix} u_1 \\ v_1 \\ w \\ u_2 \\ v_2 \end{pmatrix}, \quad \mathbf{M} = \begin{bmatrix} m_1 & 0 & 0 & 0 & 0 \\ & m_1 + m & -m & 0 & -m \\ & & m & 0 & m \\ & & & m_2 & 0 \\ sym. & & & & m + m_2 \end{bmatrix}, \quad \mathbf{C} = \begin{bmatrix} 0 & & & & 0 \\ & 0 & & & \\ & & c_g & & \\ & & & 0 & \\ 0 & & & & 0 \end{bmatrix},$$

$$\mathbf{k}(t, w) = k_g(t) f_g(w) \begin{pmatrix} 0 \\ 0 \\ 1 \\ 0 \\ 0 \end{pmatrix}, \quad \mathbf{f}_b = \begin{pmatrix} f_{x1} \\ f_{y1} \\ 0 \\ f_{x2} \\ f_{y2} \end{pmatrix} \text{ and } \quad \mathbf{f}(t) = \begin{pmatrix} F_{x1} \\ F_{y1} - F \\ F \\ F_{x2} \\ F_{y2} + F \end{pmatrix}.$$

The dynamical model represented by equation (18) is fundamentally different from model (12), in several respects. First, model (12) determines the gear shaft rotation angles completely, given the applied external moments, while in model (18) the mean angular speed of the gear shafts is pre-specified. Moreover, the gear static transmission error and the unbalance forces act as non-linear terms in equation (12) but as periodic forcing terms in equation (18). As a consequence, in the special cases where the gear backlash and the bearing non-linearities are not essential, system (18) becomes linear, since the gear meshing force is expressed in the simple form

$$f_g(\varphi_1, w, \dot{w}) = c_g\dot{w} + k_g w, \tag{19}$$

instead of equation (9), while the forces developed in each bearing are represented by the classical eight-coefficient element [10, 12] with

$$\mathbf{f}_b = \mathbf{K}_b\mathbf{u}_b + \mathbf{C}_b\dot{\mathbf{u}}_b, \tag{20}$$

instead of the non-linear form represented by equation (11). In such cases, the elements of the stiffness and damping matrices in equation (20) are evaluated by applying standard procedures [10], after determining the corresponding equilibrium position by taking into account the weight, the torque and the tooth loads applied on the gears.

4. GEARED ROTOR-BEARING SYSTEMS

In typical rotordynamic systems, gear pairs are only one of several components of the whole system. For instance, Figure 2 presents such a system, which includes a motor

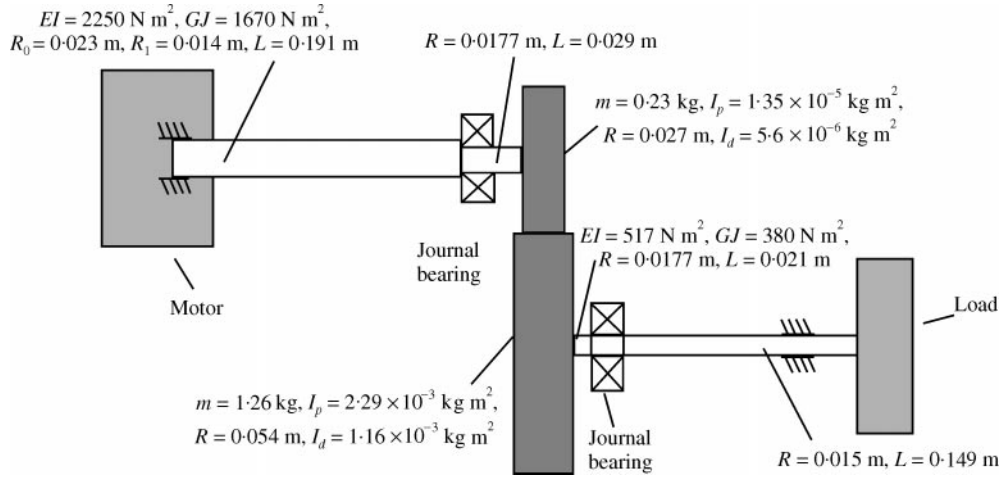

Figure 2. Mechanical model of a geared rotor-bearing system.

providing the power necessary for the function of the system, a gear-pair system as part of a gear box reducing the rotor spin speed and a load subsystem (fan, pump, propeller, generator, etc.). Here, the gear box is connected to the motor and the load subsystems through flexible shafts.

The model shown in Figure 2 is more realistic than the gear-pair system of Figure 1. On the other hand, it is also more complicated and more difficult to analyze. In fact, the order of the resulting dynamic model is so high that even the application of numerical analysis methodologies is impractical. However, there is an attractive feature of the system, which can be exploited in order to perform a systematic investigation of its dynamics; namely, the important non-linearities of the system appear in the gear mesh and the hydrodynamic bearing locations only. This localization of the non-linearities is quite common in practice and as a result, several appropriate methodologies have already appeared in the literature for such systems [15–17, 27–29]. The approach chosen in the present study for the efficient analysis of the system shown in Figure 2 is based on such methodologies and especially on that presented in reference [27]. The basic steps of this methodology are explained briefly in the remaining part of this section.

First, the system shown in Figure 2 is divided into three main components, including the driving motor and shaft (component A), the gear pair and journal bearings subsystem (component B) and the driven subsystem with its shaft (component C). Components A and C are linear and their equations of motion are obtained by applying classical finite element methodologies in the general form

$$\hat{\mathbf{M}}_A \ddot{\mathbf{u}}_A + \hat{\mathbf{K}}_A \mathbf{u}_A = \hat{\mathbf{f}}_A(t) \quad \text{and} \quad \hat{\mathbf{M}}_C \ddot{\mathbf{u}}_C + \hat{\mathbf{K}}_C \mathbf{u}_C = \hat{\mathbf{f}}_C(t) \tag{21}$$

respectively. The displacement vectors $\mathbf{u}_A$ and $\mathbf{u}_C$ include contributions from five-degree-of-freedom per node (four for the bending and one for the torsional action). Due to the linearity of the components, their matrices assume special forms. For instance, after appropriate partitioning of the displacement vector, the stiffness matrix $\hat{\mathbf{K}}_A$ may appear in the form

$$\hat{\mathbf{K}}_A = \begin{bmatrix} \hat{\mathbf{K}}_{Ax} & 0 & 0 \\ 0 & \hat{\mathbf{K}}_{Ay} & 0 \\ 0 & 0 & \hat{\mathbf{K}}_{Az} \end{bmatrix},$$

where the submatrices $\hat{\mathbf{K}}_{Ax}$, $\hat{\mathbf{K}}_{Ay}$ and $\hat{\mathbf{K}}_{Az}$ include the contribution from the bending action in the xz plane, the bending action in the yz plane and the torsional action of the driving shaft respectively.

In the above context, component B is considered as a super-element whose dynamics are governed by equations of motion similar to those presented for the gear-pair model in the previous sections. Clearly, the force developed in the gear mesh causes a coupling of the bending action in the yz planes of components A and C as well as of the torsional action in both shafts. In addition, the journal bearing of the driving shaft couples the bending action in the xz and yz planes of component A, while the journal bearing of the driven shaft causes a coupling of the bending action in the xz and yz planes of component C. Moreover, the overall coupling in the components of the total displacement vector.

$$\mathbf{u}(t) = (\mathbf{u}_A^{\mathrm{T}} \quad \mathbf{u}_C^{\mathrm{T}})^{\mathrm{T}}$$

of the composite system is enhanced further when gyroscopic effects are taken into account.

For a sufficiently accurate modelling of the overall system, the number of degrees of freedom in vector $\mathbf{u}(t)$ becomes excessively high. However, the number of degrees of freedom of components A and C can be reduced substantially, without sacrificing much accuracy, by applying a component mode synthesis methodology [16]. Through a co-ordinate transformation with the form

$$\mathbf{u}_A(t) = \mathbf{\Psi}_A \, \mathbf{q}_A(t), \tag{22}$$

the original set of equations (21a) of component A can be replaced by a considerably smaller set of equations, expressed in terms of the new generalized co-ordinates $\mathbf{q}_A$. The matrix $\mathbf{\Psi}_A$ is selected in a proper form, including free-interface normal modes and residual flexibility modes of the component (see reference [16] for details). Then, application of transformation (22) to the original set of equations (21a) yields the smaller set

$$\mathbf{M}_A \ddot{\mathbf{q}}_A + \mathbf{C}_A \dot{\mathbf{q}}_A + \mathbf{K}_A \mathbf{q}_A = \mathbf{f}_A(t), \tag{23}$$

where

$$\mathbf{M}_A = \mathbf{\Psi}_A^{\mathrm{T}} \hat{\mathbf{M}}_A \mathbf{\Psi}_A, \quad \mathbf{K}_A = \mathbf{\Psi}_A^{\mathrm{T}} \hat{\mathbf{K}}_A \mathbf{\Psi}_A \quad \text{and} \quad \mathbf{f}_A(t) = \mathbf{\Psi}_A^{\mathrm{T}} \hat{\mathbf{f}}_A(t).$$

The elements of the damping matrix $\mathbf{C}_A$ of the structural component may be selected in a way that preserves the normal modes of the corresponding undamped system [16].

The number of residual flexibility modes included in matrix $\mathbf{\Psi}_A$ is equal to the number of boundary degrees of freedom of component A. In the case examined, these degrees of freedom, say $\mathbf{q}_{AB}$, are those associated with the action of the journal bearing and the gear on the driving shaft. Consequently, the original vector of unknowns of component A is partitioned in the form

$$\mathbf{q}_A = (\mathbf{p}_A^T \quad \mathbf{q}_{AB}^{\mathrm{T}})^{\mathrm{T}}. \tag{24}$$

Analogous co-ordinate partitioning and treatment of equation (21b) leads to a similar set of equations of motion for component C. Therefore, in the final stage of the reduction processes, the equations of motion of the composite system are derived and written in the form

$$\mathbf{M}\ddot{\mathbf{q}} + \mathbf{C}\dot{\mathbf{q}} + \mathbf{K}\mathbf{q} = \mathbf{f}(t, \mathbf{q}, \dot{\mathbf{q}}) \tag{25}$$

with displacement vector

$$\mathbf{q} = (\mathbf{p}_A^{\mathrm{T}} \quad \mathbf{q}_B^{\mathrm{T}} \quad \mathbf{p}_C^{\mathrm{T}})^{\mathrm{T}}. \tag{26}$$

This synthesis step is accomplished by considering the kinetic energy, the potential energy and the virtual work of the system as a sum of the contribution from all components on these quantities [16]. For instance, for the total potential energy of the system it is true that

$$V = V_A + V_B + V_C \Rightarrow \tfrac{1}{2}\mathbf{q}^{\mathrm{T}}\mathbf{K}\mathbf{q} = \tfrac{1}{2}\mathbf{q}_A^{\mathrm{T}}\mathbf{K}_A\mathbf{q}_A + \tfrac{1}{2}\mathbf{q}_B^{\mathrm{T}}\mathbf{K}_B\mathbf{q}_B + \tfrac{1}{2}\mathbf{q}_C^{\mathrm{T}}\mathbf{K}_C\mathbf{q}_C.$$

Taking into account the displacement partitions (24), (26) and performing the necessary algebraic manipulations eventually yields the stiffness matrix $\mathbf{K}$ of the composite system. In a similar fashion, consideration of the kinetic energy and the dissipation energy yields the mass matrix $\mathbf{M}$ and the damping matrix $\mathbf{C}$ respectively. Finally, the determination of vector $\mathbf{f}(t, \mathbf{q}, \dot{\mathbf{q}})$, including the external forcing, the gear meshing force and the journal non-linearities, is most conveniently performed by evaluating the virtual work of the composite system in the form

$$\delta W = \delta W_A + \delta W_B + \delta W_C \Rightarrow$$

$$\delta\mathbf{q}^{\mathrm{T}}\mathbf{f}(t, \mathbf{q}, \dot{\mathbf{q}}) = \delta\mathbf{q}_A^{\mathrm{T}}\mathbf{f}_A(t, \mathbf{q}_A, \dot{\mathbf{q}}_A) + \delta\mathbf{q}_B^{\mathrm{T}}\mathbf{f}_B(t, \mathbf{q}_B, \dot{\mathbf{q}}_B) + \delta\mathbf{q}_C^{\mathrm{T}}\mathbf{f}_C(t, \mathbf{q}_C, \dot{\mathbf{q}}_C).$$

5. PARAMETRIC STUDY

The equations of motion of the gear pair and the rotordynamic models examined in the previous sections involve strong non-linearities, resulting from several sources. As a result, it not feasible to determine their response by means of analytical methodologies. In the general case, the dynamic response of these models can be determined by direct integration, starting from a known set of initial conditions. However, for some typical loading conditions, such as those corresponding to a constant driving moment M_{10} and a resisting moment with form

$$\hat{M}_2(\dot{\psi}_2) = \frac{M_2(\dot{\varphi}_2)}{k_0 x_c R_2} = M_{20} + \alpha\dot{\psi}_2^2, \tag{27}$$

the system response is expected to eventually become periodic. For such cases, suitable numerical methodologies exist which can determine complete branches of periodic motions, together with their stability and bifurcation properties, in a direct way.

In the numerical calculations, the two journal bearings supporting the gears are identical, with length $L = 17{\cdot}145$ mm, diameter $D = 35{\cdot}56$ mm, oil viscosity coefficient $\mu = 68{\cdot}95 \times 10^{-4}$ N s/m^2 and radial clearance $C_r = 76{\cdot}2$ μm. Here, the bearing radial clearance is chosen as the characteristic length x_c of the system. Moreover, in the nominal case the basic system parameters take the following values:

$$M_{20} = 0{\cdot}0185, \quad \alpha = 0, \quad \zeta_g = \frac{c_g}{2\sqrt{mk_0}} = 0{\cdot}05 \quad \text{and} \quad b_g = \frac{b}{C_r} = 1{\cdot}312.$$

In addition, both the gear meshing stiffness and the static transmission error are assumed to be periodic, with forms similar to those presented in reference [6]. However, the amplitude of the static transmission error is adjusted so that $\hat{e}_{c1} = 0{\cdot}05$. Also, when $\alpha \neq 0$, the numerical results are obtained by first selecting an appropriate range of values for the driving moment M_{10}. For these cases, it turns out that in the steady state

$$M_{10} = M_{20} + \alpha\Omega_2^2,$$

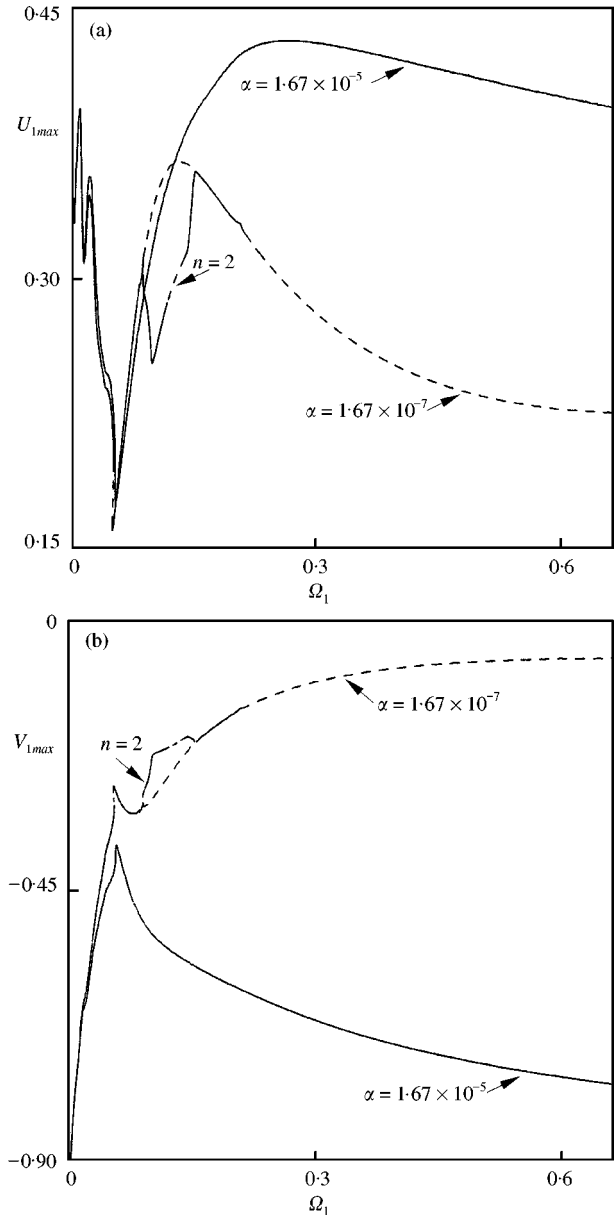

Figure 3. Effect of the spin speed dependent component of the resisting moment on steady state motions.

where Ω_2 is the average spin speed of the driven shaft, normalized by ω_0. In addition, the normalized frequency of the located periodic motions coincides with the corresponding gear meshing frequency $\Omega_M = \omega_M/\omega_0$. This makes it possible to present branches of periodic motions in the form of classical frequency-response diagrams. In these diagrams, the results are presented as a function of the normalized average spin speed Ω_1 of the driven shaft. Also, branches of stable/unstable periodic solutions are represented by solid/dashed curves respectively.

The first set of numerical results refers to gear-pair systems. In particular, Figure 3 presents response diagrams for the normalized displacements $U_1 = u_1/C_r$ and $V_1 = v_1/C_r$

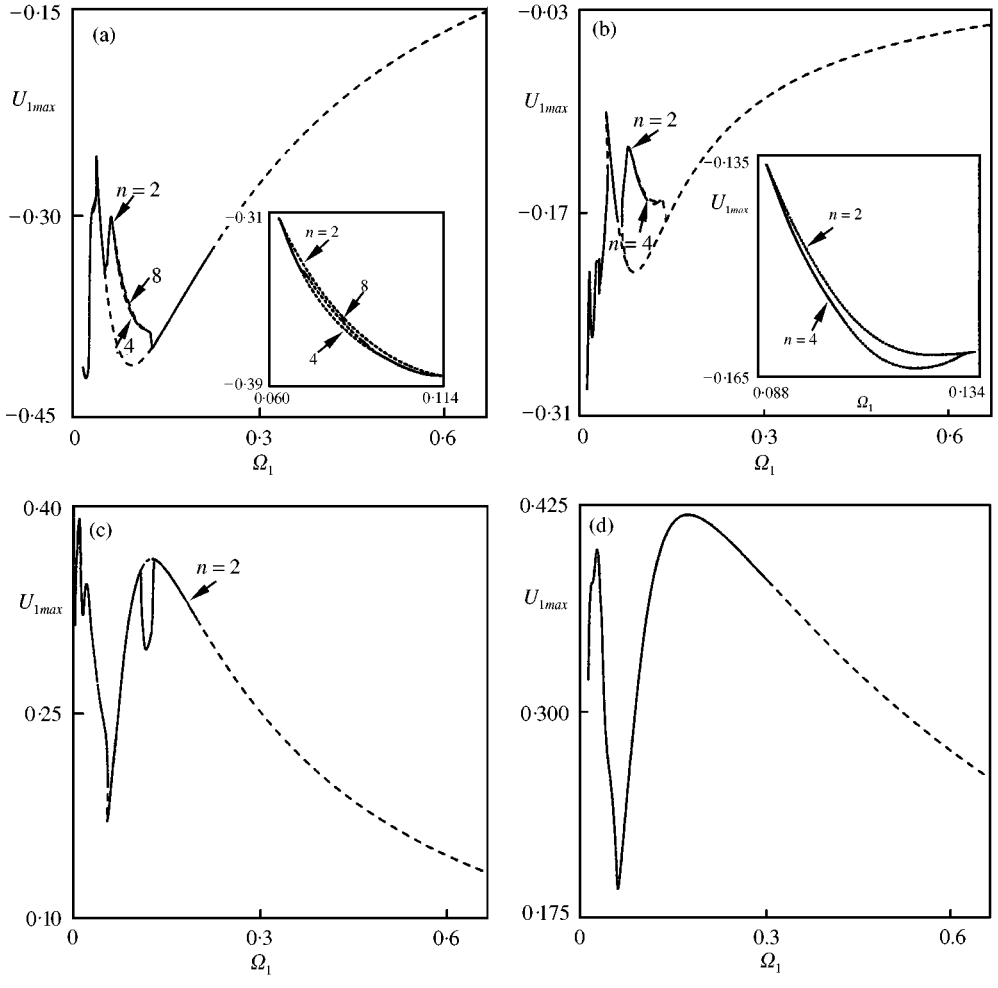

Figure 4. Effect of resisting moment amplitude on periodic motions: (a) $M_{20} = 5{\cdot}291 \times 10^{-3}$; (b) $M_{20} = 1{\cdot}0582 \times 10^{-2}$; (c) $M_{20} = 0{\cdot}0185$ and (d) $M_{20} = 0{\cdot}026455$.

of the driving gear centre for different values of the parameter α in equation (27). These results were obtained by employing the six-degree-of-freedom gear-pair model presented in section 2. As Ω_1 tends to zero, the displacement U_1 also tends to zero, corresponding to the stationary position of the gear centre. Also, in the limit $\alpha \to 0$, the results are found to virtually coincide with those obtained from the gear-pair model developed in section 3. Since the solution branches present qualitatively similar characteristics for that model, too, the effects of the other system parameters were next investigated by employing the five-degree-of-freedom model, with $\alpha = 0$.

The response diagrams of Figure 4 demonstrate the effect of the external torque amplitude on the vibration of the gear-pair model expressed by equation (18). In particular, the results for the nominal case are shown in Figure 4(c). For this case, the first branch of unstable periodic motions, obtained by increasing Ω_1 from zero, appears through saddle-node bifurcations and coexists with two other branches of stable motions. The second branch of unstable periodic motions is generated with flip bifurcations and coexists with a branch of stable $n = 2$ subharmonic motions. Finally, the third branch of unstable periodic motions arises via a Hopf bifurcation.

An increase in the amplitude of the external moment causes an elimination of the branches of unstable motions arising via saddle-node and flip bifurcations (Figure 4(d)). Moreover, the spin speed value where the Hopf bifurcation occurs is moved to higher levels. On the other hand, a decrease in the torque loads results in more interesting dynamics. Initially, the branch of stable periodic motions included between the right flip and Hopf bifurcation values decreases in size and eventually disappears (Figure 4(b)). However, a further decrease in M_{20} makes this branch reappear (Figure 4(a)). At the same time, the Hopf bifurcation spin speed value starts increasing again, while multiple branches of subharmonic motions arise via flip bifurcations in the low-frequency range. Finally, another noticeable qualitative change in the response diagrams occurs at about $M_{20} = 0{\cdot}0163$, where the static force component induced by the external moment on the driving gear is equilibrated by its weight.

In order to enhance the understanding provided by the above findings, Figure 5 presents information for the linearized gear pair model corresponding to the nominal case. More specifically, Figure 5(a) presents the undamped natural frequencies, while Figure 5(b) depicts the associated damping ratios, as a function of Ω_1. First, Figure 5(b) shows that the damping ratio of the lowest natural frequency becomes negative at about $\Omega_1 = 0{\cdot}195$, signalling the onset of instability for the linearized model. On the other hand, this is exactly the value where the $\Omega = \Omega_1/2$ (broken) line crosses the curve of the lowest natural frequency in Figure 5(a). For comparison purposes, it is noted that the Hopf bifurcation value for the nominal non-linear case was detected at $\Omega_1 = 0{\cdot}198$. Similar results were also observed for other parameter combinations. These results showed that the natural frequencies and damping ratios are affected significantly by the amplitude of the external torques. On the other hand, changes in the gear meshing stiffness and damping coefficients were found to affect only the frequency ω_v in a noticeable way.

Besides the applied torques, the systems examined may also be excited by static transmission errors and unbalances. Figure 6(a) presents results obtained by including a mass unbalance of $e = 10$ μm in the driving gear (curve 1), together with results obtained for a case with no unbalance and a static transmission error with amplitude 3 times smaller than the nominal (curve 2). Obviously, a reduction in the loading caused by static transmission errors and unbalances attenuates the effect of the non-linearities. Furthermore, when both the unbalance and the static transmission error are negligible, the response diagram takes the form shown in Figure 6(b). Here, the absence of external loading allows constant solutions of the equations of motion to appear represented by the thinner lines. Also, the branch of unstable periodic motions emanates from them at a subcritical Hopf bifurcation point. These periodic solutions involve a hysteresis, they become stable via a saddle-node bifurcation and their amplitude becomes relatively large (in fact, it quickly approaches the bearing radial clearance), in accordance with experimental observations [13, 20].

To gain a deeper insight into the gear-pair dynamics, Figure 7(a) depicts the lower undamped natural frequencies of the linearized system corresponding to Figure 6(b), as a function of Ω_1. Moreover, the broken and dashed curves represent similar quantities of the driving and driven gear systems, respectively, when they are decoupled from each other (i.e., for $k_g = 0 = c_g$). Finally, the thicker curve indicates the frequency of the branch of periodic motions. At the Hopf bifurcation point, this frequency is almost half the value of the driving shaft spin speed. It then becomes smaller, but in a slower fashion than that observed in similar but single-shaft systems [15]. These results, in conjunction with those presented in Figure 5, indicate that the onset of instability of the geared system examined occurs at a spin speed Ω_1, which is about twice the lowest natural frequency of the linearized model. This is in agreement with similar observations for single-shaft systems on journal bearings

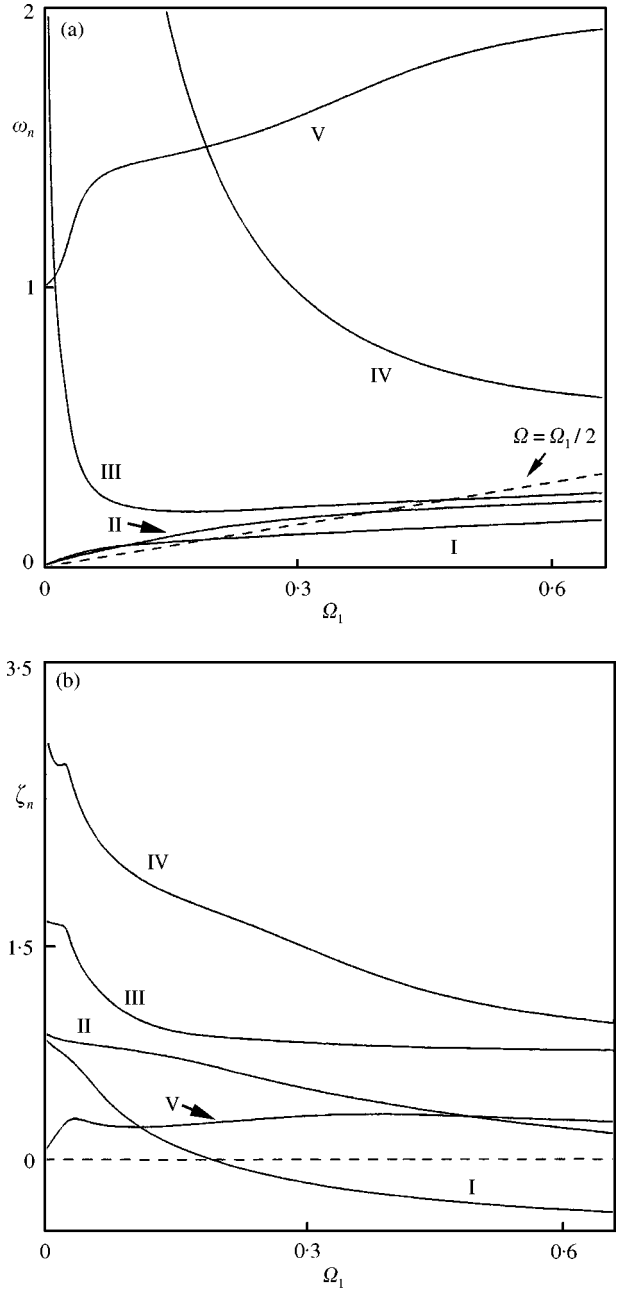

Figure 5. Eigenvalues of linearized nominal model as a function of spin speed: (a) undamped natural frequencies and (b) damping ratios.

[13, 15]. However, in some other cases, this instability is not necessarily related directly to the lowest natural frequency of the system, as shown in Figure 7(b).

The following sequence of diagrams illustrates differences observed in the response by considering more deviations from the nominal case. First, Figure 8(a) presents results obtained for the linearlized nominal model (curve 1) or by using short instead of finite

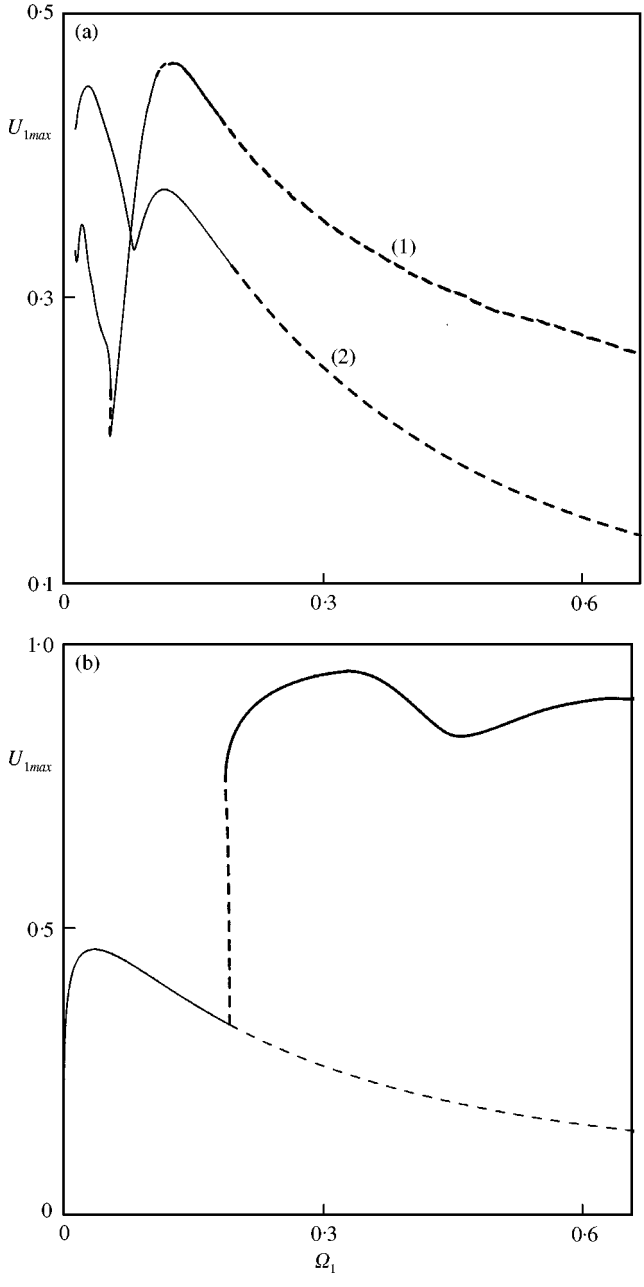

Figure 6. Effect of loading parameters: (a) system with an unbalance of $e = 10\ \mu$m (curve 1) and system with static transmission error (curve 2) and (b) system with no unbalance and static transmission error.

bearing theory (curve 2). In the first case, the most important differences are recorded in the low-frequency range, where both primary and subharmonic resonances are captured in Figure 4(c). In contrast, the results from the short bearing theory deviate from those of the finite bearing theory throughout the frequency range examined, since the ratio L/D of the bearings is 0·48, which lies within the validity limit of short bearing theory [10].

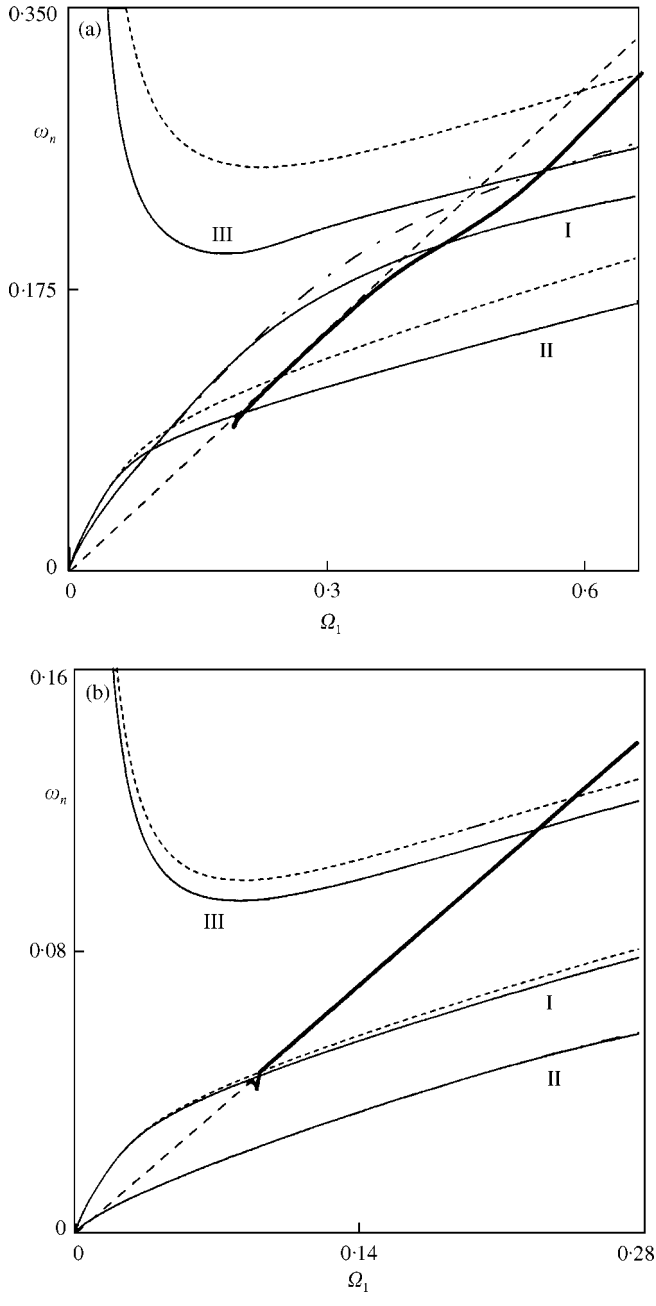

Figure 7. Undamped natural frequencies for: (a) $R_2 = 2R_1$ (nominal case); (b) $R_2 = 5R_1$.

Likewise, the effect of the oil viscosity coefficient of the journal bearings is illustrated in Figure 8(b). Among other things, a decrease in the value of this parameter, caused by a temperature rise, leads to an increase in the critical spin speed, which is in accordance with earlier experimental observations [20]. On the other hand, the effect of decreasing the value of the gear meshing damping ratio has more important implications in the low-frequency range, as shown in Figure 8(c). Finally, the effect of the gear backlash is also more

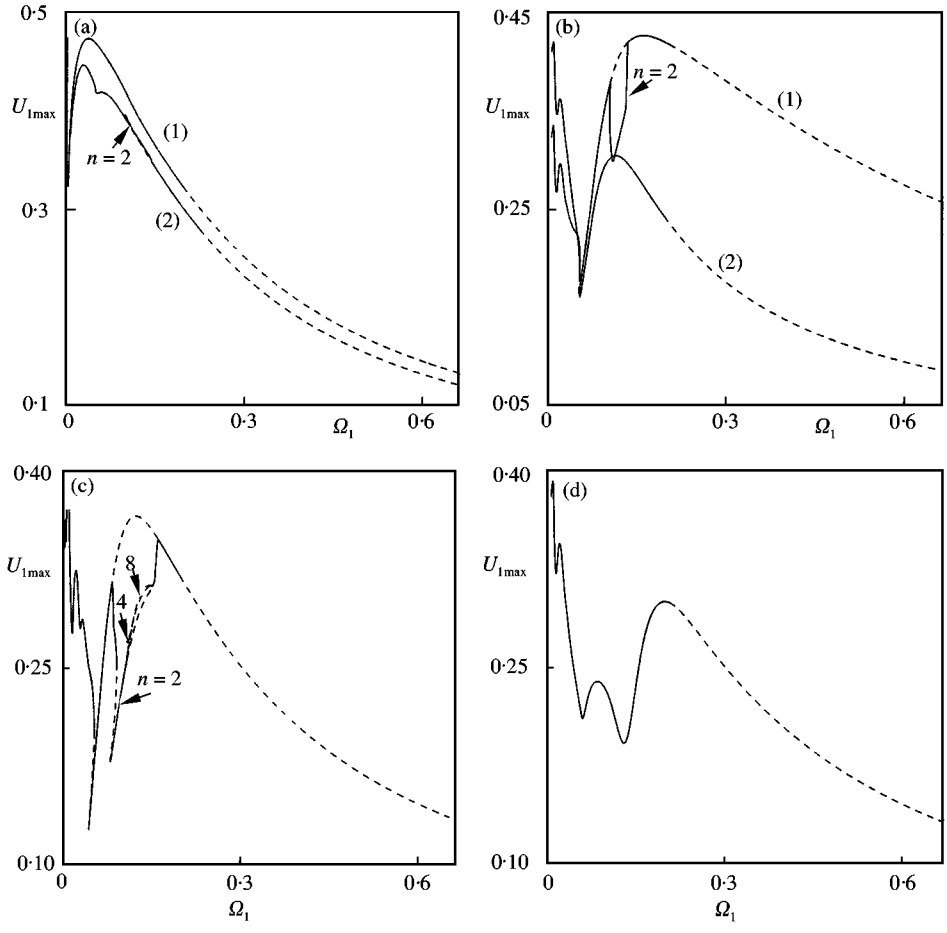

Figure 8. Frequency–response diagram obtained for: (a) the linearized model (curve 1) and by application of short bearing theory (curve 2); (b) oil viscosity coefficient $\mu = 30 \times 10^{-4}$ N s/m^2 (curve 1) and 110×10^{-4} Ns/m^2 (curve 2); (c) gear mesh damping $\zeta_g = 0{\cdot}005$ and (d) zero gear backlash.

pronounced in the low-frequency regime. This is demonstrated in Figure 8(d), which was obtained by neglecting the gear backlash (i.e., for $b_g = 0$).

Application of the present methodology leads to direct evaluation of the loads induced on the gear teeth during operation. Figure 9(a) presents the maximum value of the force developed at the gear mesh, expressed in the form of equation (9) and normalized by the static value M_{10}/R_1, as a function of Ω_1, for the nominal case. Likewise, the results of Figure 9(b) were obtained after assuming that the gear meshing damping becomes zero (instead of remaining constant) when the gear teeth lose contact (i.e., when $|w| < b$). The main differences between these two cases are observed in the vicinity of the lowest and the middle unstable regimes. However, in both cases there is a great deviation from the corresponding static value of one. This illustrates the large errors involved in models that adopt the common "side load" approach. This conclusion is reinforced further by inspecting the complicated time histories obtained over a response period, shown in the insets at selected spin speeds. The fact that the meshing force may be much larger than the corresponding static value has significant practical implications, related to the fatigue strength of the gear teeth.

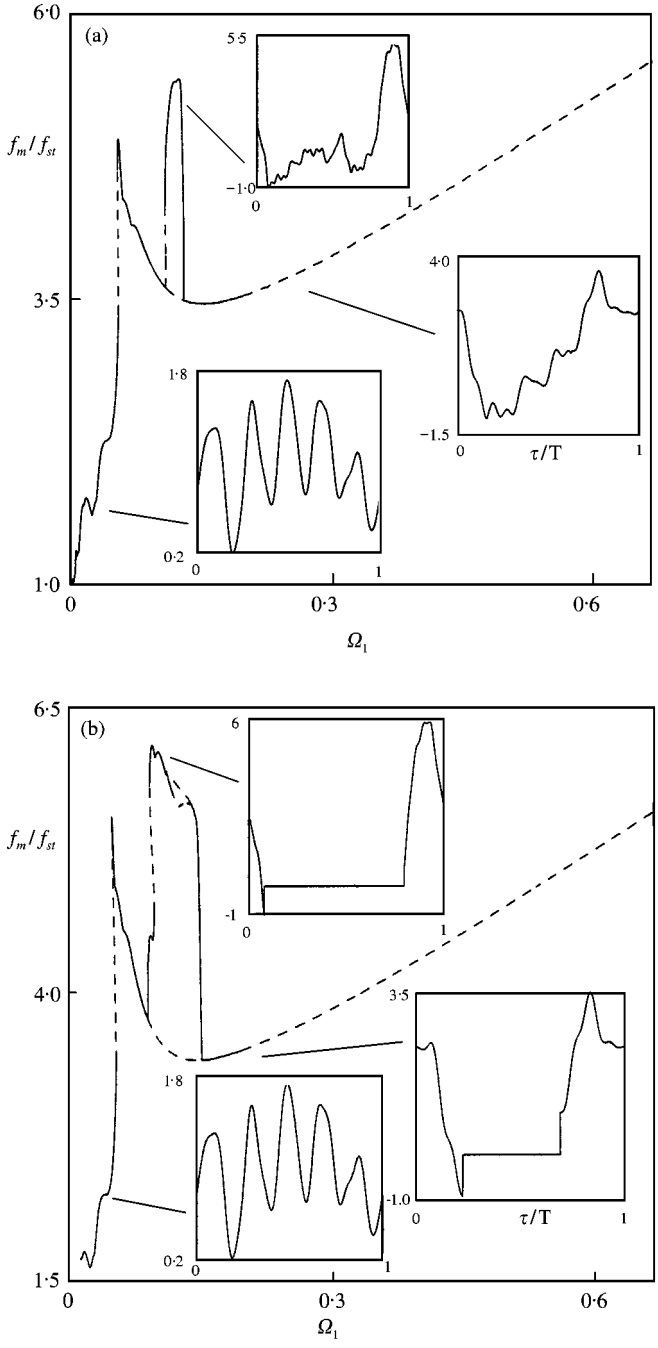

Figure 9. Amplitude of force developed at the gear mesh for: (a) linear mesh damping and (b) non-linear mesh damping.

In the final part of this section, some characteristic numerical results are presented for a typical rotordynamic system with flexible shafts. Here, the emphasis is placed on demonstrating the validity and effectiveness of the methodology described in section 4, rather than on obtaining another exhaustive set of numerical results. The system shown in

TABLE 1

Natural frequencies of linearized model at $\Omega_1 = 0{\cdot}207$

Complete model	Reduced model
0	0
0·084	0·084
0·151	0·151
0·161	0·161
0·175	0.175
0·422	0·422
0·426	0·426
0·459	0·459
0·557	0·556
0·911	0·911
0·941	0·941
0·995	0·995
1·076	1·076
1·260	1·261
3·017	3·031
3·027	3·116
3·158	4·174
3·892	5·122

Figure 2 is examined and its shafts are modelled by beam finite elements. In the reduction stage, component A was represented by three rigid-body modes, five free interface flexible modes and five boundary degrees of freedom, while component C was represented by an identical number of modes. As a result, the reduced system consisted of 26 degrees of freedom.

The accuracy of the component mode synthesis method is first verified by the results of Table 1, presenting the lower natural frequencies of the reduced and complete linearlized nominal system, at a specific spin speed. Direct comparison shows that the differences between the first 14 frequencies of the complete and the reduced model are negligible. This level of accuracy is controlled by the number of flexible modes included in the reduced model and is maintained throughout the frequency range of interest. These findings are further reinforced by the response diagrams of Figure 10. In particular, Figure 10(a) shows the overall lateral displacement of the driving gear centre, while Figure 10(b) presents its deviation from the corresponding static value. Again, the results obtained for the reduced system (curve 1) are virtually identical and cannot be distinguished from the results obtained for the corresponding complete model (curve 2), within the frequency range of interest. Finally, curve 3 presents a similar diagram, obtained after including the gyroscopic effects associated with the motor, load and gear elements.

6. DIRECT INTEGRATION OF THE EQUATIONS OF MOTION

In the great majority of the response diagrams presented in the previous section frequency ranges exist where no stable steady state motion is captured. For instance, two such frequency intervals appear in Figure 8(c). In order to develop a more complete picture for the system response, the dynamics in these ranges are next investigated further, by direct integration of the equations of motion (18).

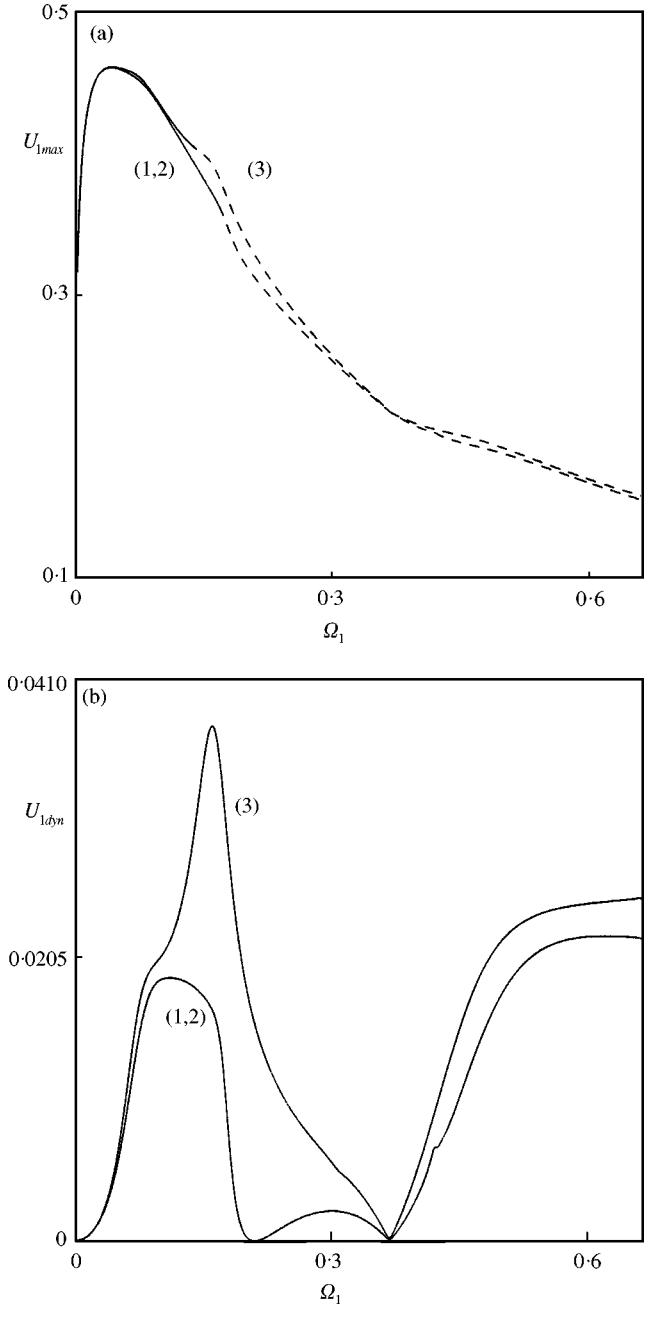

Figure 10. Response diagrams for a geared rotor-bearing system (curve 1: reduced model, curve 2: complete model and curve 3: model including gyroscopics): (a) comparison of overall lateral displacement at the driving gear and (b) comparison of dynamic component of lateral displacement.

First, the dynamics within the low-frequency range shown in the inset of Figure 8(c), are dominated by a sequence of period-doubling bifurcations. As a consequence, the orbits of the driving gear appear in the form shown in Figure 11, for several values of the spin speed Ω_1. As usual, following a finite number of observable period doublings, the system settles

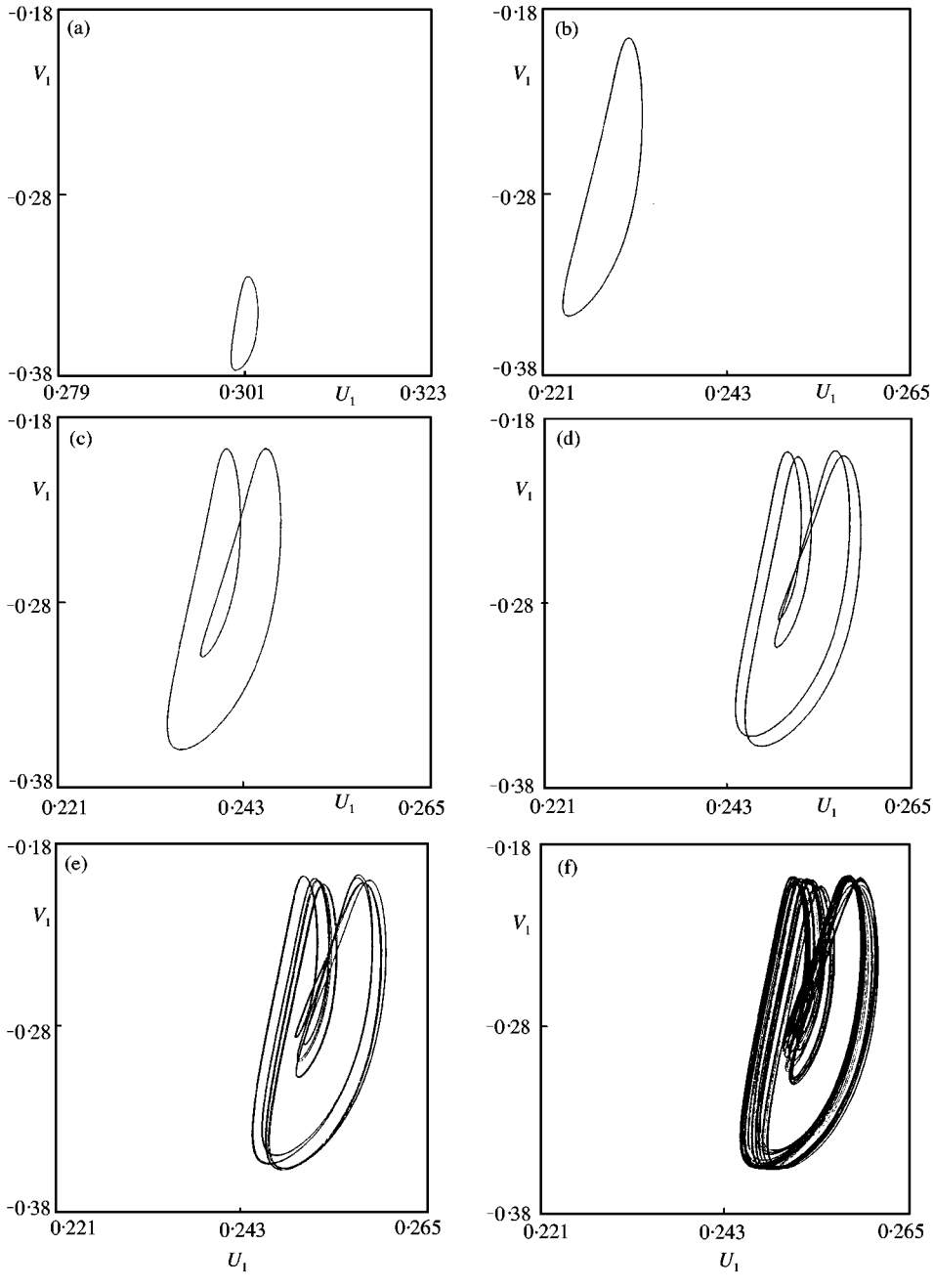

Figure 11. Orbits of the driving gear centre in the vicinity of the flip bifurcations: (a) $\Omega = 0{\cdot}08$; (b) 0·1; (c) 0·1053; (d) 0·1093; (e) 0·1096 and (f) 0·11.

eventually into a chaotic response [19]. The trajectories obtained may occasionally appear in a rather complicated form. However, throughout the frequency interval of interest, the displacement amplitudes were found to remain close to those of the coexisting unstable periodic motion.

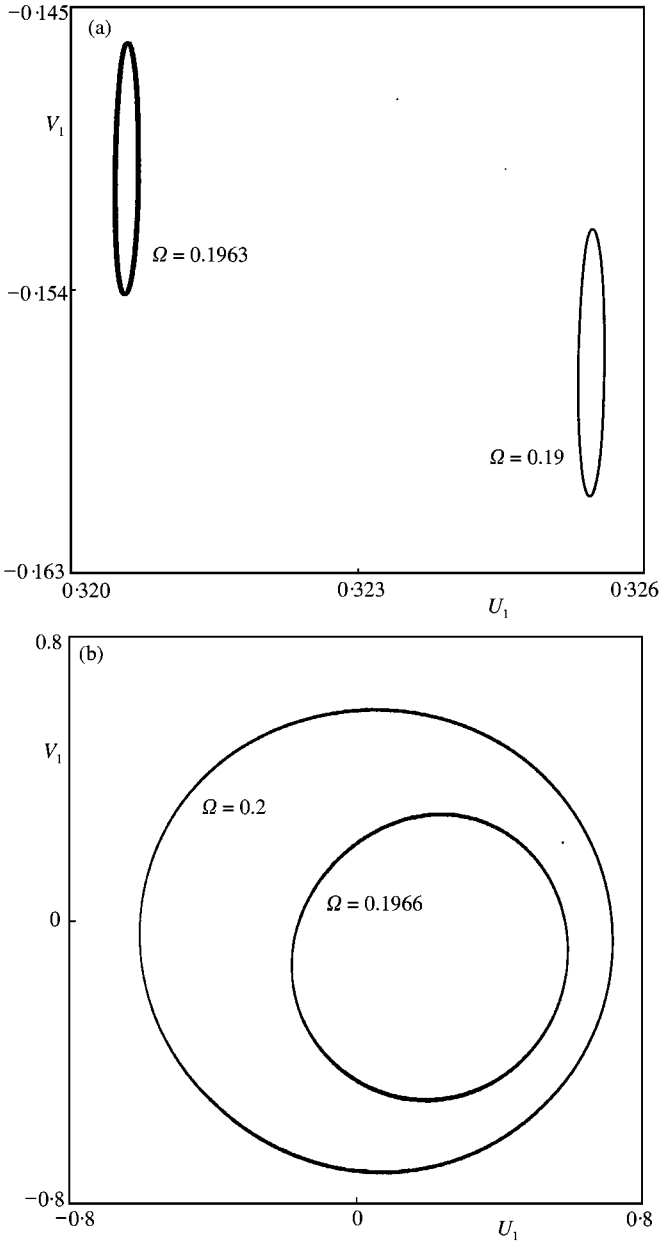

Figure 12. Orbits of the driving gear centre in the vicinity of the Hopf bifurcation: (a) $\Omega = 0{\cdot}19$ and $0{\cdot}1963$; (b) $\Omega = 0{\cdot}1966$ and $0{\cdot}2$.

A quite different response scenario was observed in the high-frequency unstable regime of Figure 8(c). Following the Hopf bifurcation, the original periodic motion is initially replaced by a quasi-periodic motion with comparable displacement amplitudes (Figure 12(a)), as usual [19]. However, this motion is very quickly replaced by motions with much higher response amplitudes (Figure 12(b)). In fact, these new motions were found to persist throughout the high-frequency interval and have amplitudes close to the bearing radial clearance. This transition presents many similarities with the amplitude changes

observed in Figure 6(b), when the unforced system undergoes a rapid transition from constant to high amplitude periodic motions. Moreover, it also appears to follow the pattern of similar instabilities observed in single-shaft systems with journal bearings [13, 15].

The results from direct integration, in conjunction with the results presented in the previous section, shed light on and help in explaining some earlier experimental observations [20]. For instance, the response diagrams of Figure 4 illustrate the strong influence of the external loading on the response amplitudes and stability. Therefore, depending on the loading level, the same system may exhibit quite different behaviour as the spin speed of its shafts is increased gradually. More specifically, for relatively large loading the system will exhibit large-amplitude motions, characterized as oil whirl and then oil whip instability, only immediately after the Hopf bifurcation value. However, for lower loading levels, the same system may first pass through spin speed intervals where subharmonic motions occur, like the single-shaft systems [13]. These motions belong to $n = 2$ branches, mainly, but they can evolve to become even chaotic. However, their amplitude is always comparable with the amplitude of the coexisting but unstable $n = 1$ motion. This is exactly what distinguishes these motions from those occurring after the Hopf bifurcation.

7. SYNOPSIS AND CONCLUSIONS

A systematic methodology has been developed for determining the dynamic behaviour of geared rotordynamic systems supported on oil journal bearings. Initially, models of simple gear-pair systems were set-up, including effects from gear mesh backlash and damping, static transmission error, unbalances and external torques. In particular, the gear meshing stiffness and the static transmission error were modelled as periodic functions of the gear rotation. The resulting equations of motion include strong non-linearities, arising from the gear meshing and the journal action. This makes the application of analytical methods unfeasible and as a consequence, an effective numerical methodology was developed for obtaining their steady state response and stability properties. Then, systems with flexible shafts were also considered. The shafts were modelled with finite elements, while the gear-pair was included as a super-element. By application of a component mode synthesis method, the system order can be reduced to sizes that can be treated by the methodology applied to the gear-pair models.

In the last part of the study, numerical results were presented, providing a better understanding of the dynamics related to the interaction of the gear meshing and the oil journal non-linearities. This was achieved through sequences of response diagrams, which in conjunction with results from direct integration of the equations of motion, revealed the effect of the system parameters on its response and stability properties. More specifically, from the response diagrams it was first noticed that the systems examined may possess several branches of unstable periodic response, generated through flip or Hopf bifurcations. The former occur at relatively low spin speeds and may lead to quasi-periodic or chaotic response with amplitudes comparable to those of the coexisting unstable periodic motion. In contrast, the Hopf bifurcation appears at higher spin speeds and leads to motions with substantially greater amplitudes. These phenomena present many similarities as well as some differences compared with phenomena observed for single-shaft systems on journal bearings.

Among all the parameters, the magnitude of the external torques was found to play a dominant role in the system dynamics. For instance, an increase in these torques caused elimination of the period-doubling bifurcations and moved the Hopf bifurcation to higher

speeds. On the other hand, a reduction of the external torques led to more interesting dynamics. In particular, the onset of the Hopf instability for systems with negligible static transmission error and unbalance was found to occur at a spin speed which is about twice that of the lowest natural frequencies of the corresponding linearized model. However, the frequency of the resulting periodic motion was smaller but remained close to half the value of the spin speed, in all cases examined. Finally, the effect of other parameters, like the gear meshing damping, backlash and oil viscosity, was also investigated. In addition, apart from predicting displacement amplitudes and capturing orbits at selected points, the force developed at the gear mesh was also evaluated and it was verified that its amplitude may be much larger than the corresponding static value.

REFERENCES

1. J. W. LUND 1978 *Journal of Mechanical Design* **100**, 535–539. Critical speeds, stability and response of a geared train of rotors.
2. H. LIDA, A. TAMURA, K. KIKUCH and H. AGATA 1980 *Bulletin of the JSME* **23**, 2111–2117. Coupled torsional–flexural vibration of a shaft in a geared system of rotors.
3. S. V. NERIYA, R. B. BHAT and T. S. SANKAR 1985 *The Shock and Vibration Bulletin* **55**, 13–25. Coupled torsional–flexural vibration of a geared shaft system using finite element analysis.
4. H. H. LIN, R. L. HUSTON and J. J. COY 1988 *American Society of Mechanical Engineers Journal of Mechanisms, Transmissions and Automation in Design* **110**, 221–229. On dynamic loads in parallel shaft transmissions (parts I and II).
5. F. K. CHOY, Y. K. TU, J. J. ZAKRAJSEK and D. P. TOWNSEND 1991 *American Society of Mechanical Engineers Journal of Vibration of Acoustics* **113**, 333–334. Effects of gear box vibration and mass imbalance on the dynamics of multistage gear transmission.
6. A. KAHRAMAN and R. SINGH 1991 *Journal of Sound and Vibration* **146**, 135–156. Interactions between time-varying mesh stiffness and clearance nonlinearities in a geared system.
7. C. PADMANABHAN and R. SINGH 1996 *Journal of the Acoustical Society of America* **99**, 324–334. Analysis of periodically forced nonlinear Hill's oscillator with application to a geared system.
8. F. PFEIFFER and C. GLOCKER 1996 *Multibody Dynamics with Unilateral Contacts*. New York: Wiley-Interscience.
9. S. THEODOSSIADES and S. NATSIAVAS 2000 *Journal of Sound and Vibration* **229**, 287–310. Nonlinear dynamics of gear-pair systems with periodic stiffness and backlash.
10. D. CHILDS, H. MOES and H. VAN LEEUWEN 1977 *American Society of Mechanical Engineers Journal of Lubrication Technology* **99**, 198–210. Journal bearing impedance descriptions for rotordynamic applications.
11. E. J. GUNTER, L. E. BARRETT and P. E. ALLAIRE 1977 *American Society of Mechanical Engineers Journal of Lubrication Technology* **99**, 57–64. Design of nonlinear squeeze-film dampers for aircraft engines.
12. M. L. ADAMS 1980 *Journal of Sound and Vibration* **71**, 129–144. Nonlinear dynamics of flexible multi-bearing rotors.
13. A. MUSZYNSKA 1986 *Journal of Sound and Vibration* **110**, 443–462. Whirl and whip—rotor/bearing stability problems.
14. M. M. KHONSARI and Y. J. CHANG 1993 *American Society of Mechanical Engineers Journal of Vibration and Acoustics* **115**, 303–307. Stability boundary of nonlinear orbits within clearance circle of journal bearings.
15. E. L. B. VAN DE VORST, R. H. B. FEY, A. DE KRAKER and D. H. VAN CAMPEN 1996 *Nonlinear Dynamics* **11**, 295–313. Steady-state behavior of flexible rotordynamic systems with oil journal bearings.
16. R. R. CRAIG, Jr 1981 *Structural Dynamics—An Introduction to Computer Methods*. New York: John Wiley & Sons.
17. H. D. NELSON, W. L. MEACHAM, D. P. FLEMING and A. F. KASCAK 1983 *American Society of Mechanical Engineers Journal of Power Engineering* **105**, 606–614. Nonlinear analysis of rotor-bearing systems using component mode synthesis.
18. E. DOEDEL 1986 *AUTO: Software for Continuation and Bifurcation Problems in Ordinary Differential Equations*. Pasadena, CA: California Institute of Technology.

19. A. H. NAYFEH and B. BALACHANDRAN 1995 *Applied Nonlinear Dynamics*. New York: John Wiley & Sons.
20. T. YAMADA and J. MITSUI 1979 *Bulletin of the JSME* **22**, 98–106. A study on the unstable vibration phenomena of a reduction gear system, including the lightly loaded journal bearings, for a marine steam turbine.
21. H. R. SIMMONS and A. J. SMALLEY 1984 *American Society of Mechanical Engineers Journal of Engineering for Gas Turbine and Power* **106**, 946–951. Lateral gear shaft dynamics control torsional stresses in turbine-driven compressor train.
22. P. SCHWIBINGER and R. NORDMANN 1988 *American Society of Mechanical Engineers Journal of Engineering for Gas Turbine and Power* **110**, 563–571. The influence of torsional-lateral coupling on the stability behavior of geared rotor systems.
23. B. KISHOR and S. K. GUPTA 1989 *American Society of Mechanical Engineers Journal of Vibration, Acoustics and Reliability in Design* **111**, 234–240. On the dynamic analysis of a rigid rotor–gear pair-hydrodynamic bearing system.
24. C.-S. CHEN, S. NATSIAVAS and H. D. NELSON 1998 *American Society of Mechanical Engineers Journal of Vibration and Acoustics* **120**, 860–867. Coupled lateral-torsional vibration of a gear-pair system supported by a squeeze film damper.
25. C.-S. CHEN, S. NATSIAVAS and H. D. NELSON 1997 *American Society of Mechanical Engineers Journal of Vibration and Acoustics* **119**, 85–88. Stability analysis and complex dynamics of a gear-pair system supported by a squeeze film damper.
26. N. G. ARAKERE and C. NATARAJ 1999 *American Society of Mechanical Engineers Design Engineering Technical Conferences*. Las Vegas, Nevada. Numerical simulation of nonlinear spur gear dynamics.